

1 **Evolution of Sea Surface Temperature in the Southern Mid-latitudes from Late Oligocene**  
2 **through Early Miocene**

3 **José Guitián<sup>1</sup> and Heather M Stoll<sup>1</sup>**

4 <sup>1</sup>Geological Institute, ETH Zürich, Switzerland

5 Corresponding author: José Guitián ([jose.paleocean@gmail.com](mailto:jose.paleocean@gmail.com))

6 **Key Points:**

- 7     • Alkenone-derived Sea Surface Temperatures from the Tasmanian Sea show cold  
8     conditions related with the MOGI.
- 9     • Despite the latitudinal drift of the site, the record confirms the long term warming  
10    during the Late Oligocene and a colder Early Miocene.
- 11    • This record highlights the different amplitudes of Late Oligocene warming obtained  
12    from different proxies and locations.

## 13 **Abstract**

14 Large Antarctic ice volume changes characterized the middle to Late Oligocene and the first  
15 million years of climate evolution during the Miocene. However, the sea surface temperature  
16 (SST) evolution over this period remains poorly constrained, as only a few records from  
17 contrasting proxies are available. In this study, we present a long-term alkenone-derived SST  
18 record from sediments drilled by the Ocean Drilling Program (ODP) at Site 1168 in the west  
19 Tasmanian Sea spanning 29.8 Ma to 16.7 Ma. The SST record highlight that the long-term  
20 warming in the Late Oligocene linked to the end of the Middle Oligocene Glacial Interval can  
21 be recognized also at mid-to-high latitudes of the Southern Hemisphere. Warmer average  
22 temperatures (25.5°C) characterize the period from 24.6 to 22 Ma; average temperatures then  
23 decrease by 1 to 2°C into the Miocene and stabilize by 20.1 Ma. The reconstructed temperatures  
24 are highly variable in the warm Late Oligocene waters, and more stable and slightly colder in  
25 the Early to Middle Miocene. We confirm that this temperature trend is not an artefact of the  
26 latitudinal drift of the site, as the temperature anomaly relative to the modern water temperature  
27 at the paleolocation confirms the SST trends of the Oligocene. This is the first alkenone-derived  
28 record to reproduce the long-term Oligocene climate trend previously interpreted from the  
29 benthic  $\delta^{18}\text{O}$ , which recorded a warming and/or reduction in ice volume from the Middle  
30 Oligocene Glacial Interval through the latest Oligocene.

## 31 **1. Introduction**

32 Suborbital resolution deep-sea benthic oxygen isotope records reveal large oscillations, at both  
33 orbital and multimillion-year timescales, over the Oligocene to Early Miocene time interval (De  
34 Vleeschouwer et al., 2017; Westerhold et al., 2020; Zachos et al., 2008) which are interpreted  
35 to reflect large variations in the Antarctic ice volume and temperature oscillations at the deep-  
36 water formation regions (Liebrand et al., 2017; Pekar and DeConto, 2006). The Oligocene  
37 presents a 2.5 myr long period of enriched  $\delta^{18}\text{O}$  described as the Middle Oligocene Glacial  
38 Interval (MOGI) (Liebrand et al., 2017), followed by a long term shift towards lighter values  
39 from 26.5 Ma attributed to a Late Oligocene Warming (LOW) (Pekar et al., 2006; Villa and  
40 Persico, 2006). Some interpretations propose that the variation in benthic  $\delta^{18}\text{O}$  signal is  
41 dominantly driven by ice volume, rather than deep-sea temperature (Liebrand et al., 2017).  
42 However, this deep-sea interpretation of climate has not yet been widely contrasted with long  
43 term and sea surface temperature (SST) records from mid to high latitude regions, which leaves  
44 the global SST reconstructions versus ice volume interpretation unclear.

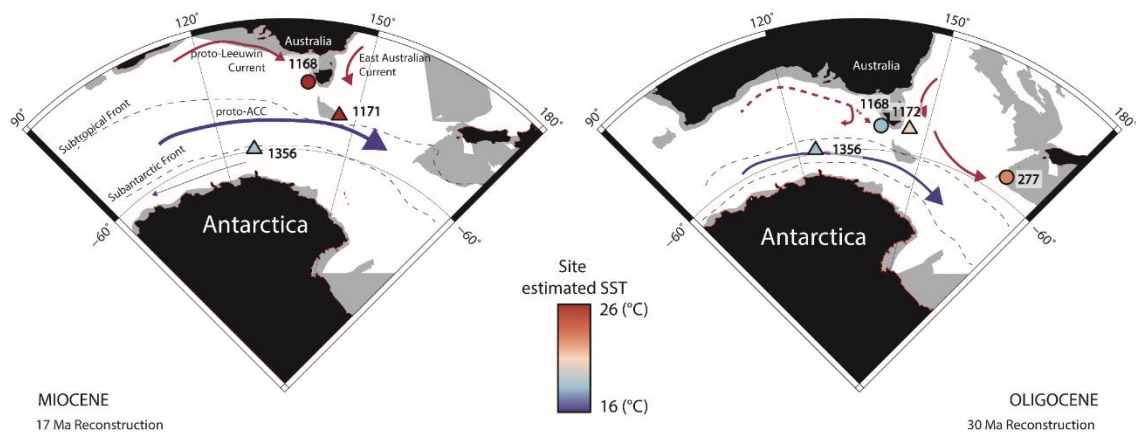
45 The majority of available SST records spanning the Oligocene and Miocene are based on  
46 organic biomarkers, glycerol dialkyl glycerol tetraethers (GDGTs) TEX<sub>86</sub> index and these  
47 present some paradoxes. GDGT-based estimates suggest similar absolute temperature at two  
48 tropical sites (O'Brien et al., 2020; Zhang et al., 2013) as at mid-to high latitude sites in the  
49 North and South Atlantic Ocean (O'Brien et al., 2020; Super et al., 2018), an absence of  
50 temperature gradients difficult to reconcile with climate models. While some of these records  
51 suggest long-term SST trends superimposed on higher frequency variability, GDGTs-derived  
52 temperatures from the Southern Ocean high latitude Site 1356 do not resolve multimillion year  
53 trends such as the MOGI or the Late Oligocene warming (Hartman et al., 2018) but do suggest  
54 high amplitude SST changes over orbital timescales starting at the Early Oligocene.

55 The few long-term SST records for the Oligocene to Early Miocene estimated from the long-  
56 chain alkenone unsaturation ratio ( $U_{37}^{k'}$ ) are restricted to mid latitude sites in the North Atlantic,  
57 where they define punctuated excursions and multimillion-year variations coincident with the  
58 benthic isotope records (Gutián et al., 2019; Liu et al., 2018). However, these records are  
59 interrupted during part of the MOGI and during the Early Miocene, potentially underestimating  
60 the amplitude of its temperature change.

61 Therefore, additional SST reconstructions are required to explore the temperature variability at  
62 mid-to-high latitude sites, especially in the Southern Ocean, the region most proximal to the  
63 main polar ice cap in the Oligocene. To this end, this study presents a new alkenone-based SST  
64 record from  $U_{37}^{k'}$  index over the Middle Oligocene to Early Miocene using sediments recovered  
65 from the West South Tasmanian Rise by the Ocean Drilling Program (ODP) at Site 1168 which  
66 had a estimated paleolatitude of 54°S by the middle Oligocene (Exon et al., 2001), ideal for  
67 providing a mid-latitude Southern Hemisphere view on surface ocean temperature. Our goal is  
68 to evaluate at this location whether there is a clear SST manifestation of the MOGI and LOW  
69 which were interpreted from global benthic  $\delta^{18}\text{O}$ . Although the relationship between ice  
70 volume and polar temperatures is complex (cite Bradshaw et al 2021, Evans et al 2021), recent  
71 models have proposed that large changes in the aerial coverage of Antarctic ice sheet do lead  
72 to coupled changes in SST around Antarctica which contribute to changing deep-sea  
73 temperature and benthic  $\delta^{18}\text{O}$ . Thus, although not providing a hard constraint on deep-water  
74 temperatures, our results can help assess the likelihood of an exclusively ice volume, vs  
75 combined ice volume and deep-sea temperature contribution to the amplitude of benthic  $\delta^{18}\text{O}$   
76 at this time.

77 The sediments of ODP 1168 preserve abundant biomarkers through the Oligocene and early  
78 Miocene. In this period, ODP 1168 transitions from carbonate-poor claystone to clay-bearing  
79 carbonate rich sediments related to deepening of the basin. Application of recent analytical  
80 techniques allow better separation of both  $C_{37}$  and  $C_{38}$  long chain alkenones (Longo et al., 2013)  
81 to identify alkenone indices that verify  $U_{37}^{k'}$ -calculated SST trend despite the change in coastal  
82 proximity of the site where different alkenone producer populations may have different  $U_{37}^{k'}$  to  
83 temperature calibrations (D'Andrea et al., 2016). The site location on the Tasmanian Rise was  
84 influenced by the gradual northward movement of the Australian plate, which widened the  
85 gateway between Australia and Antarctica and strengthened the exchange of water masses  
86 between the south Pacific and the Indian Ocean (Exon et al., 2002; Pfuhl and McCave, 2005;  
87 Pfuhl et al., 2004; Scher et al., 2015; Stickley et al., 2004b). We account for this latitudinal  
88 movement in the examination of temperature trends and gradients. Our SST record has an  
89 average 350 ky resolution, and although it exhibits high frequency variation potentially related  
90 to orbital cycles, coherent significant multi-million year scale trends in mean SST are evident.  
91 Biostratigraphic and magnetostratigraphic constraints on the age model allow us to compare  
92 our records with the existing SST reconstructions in the Southern Ocean to explore the  
93 evolution of temperature gradients, as well as with globally distributed SST estimates and high  
94 resolution benthic  $\delta^{18}\text{O}$  from other sites.

## 2. Setting and sediments



96

97 **Figure 1.** Reconstructed map of the study area with inferred surface ocean currents (red and  
 98 blue solid and dashed lines) and convergent fronts (black dashed lines) (Salabarnada et al.,  
 99 2018; Scher et al., 2015). Black fill denotes the paleo-location of the currently exposed  
 100 continental area while the grey shading shows the continental rise. Site locations are shown  
 101 with triangles and circles for GDGT-derived and alkenone-derived SST respectively, and are  
 102 coloured as a function of the estimated paleotemperature at each timeslice after published SST  
 103 estimates (Hartman et al., 2018; Houben et al., 2019; Leutert et al., 2020; Liu et al., 2009)  
 104 (Table S1).

105 Site ODP 1168 is located in the offshore of the Australian plate at the western margin of  
 106 Tasmania (Figure 1), at 43° 36.57'S and 139 144° 24.76'E, and 2463m water depth, drilled  
 107 within a graben-developed basin with sediment accumulation since the latest Eocene (Exon et  
 108 al., 2001). It is one of the few locations in mid paleolatitudes with relatively carbonate rich  
 109 sequences for this time interval (Exon et al., 2001).

110 During the Late Eocene the area was within a system of migrating deltas and relatively restricted  
 111 basins (Exon et al., 2001) which then led to a progressive deepening to 2.5 km by the end of  
 112 the Miocene (Exon et al., 2001; Hill and Exon, 2004; Stickley et al., 2004b) as a consequence  
 113 of the northward shift of the Australian continent. For the interval in our study, a recent  
 114 synthesis of data including seismic stratigraphy suggest deepening from a paleodepth of about  
 115 700 m at 29 Ma to a depth of 1500 m for Site 1168 area by 21 Ma (Hochmuth et al., 2020). The  
 116 deltaic coastline systems along the western Tasmanian continental margin and nearby isolated  
 117 islands were most likely the source of material deposited at Site 1168 over the Early Oligocene  
 118 (Exon et al., 2001; Hochmuth et al., 2020). Although carbonate content and preservation of  
 119 biogenic calcite start to increase along the Early Oligocene, C/N ratios suggest that terrestrial  
 120 organic matter input was predominant before 30.5 Ma (Exon et al., 2001). The lines of evidence  
 121 suggest that, the gradual subsidence and increasing distance from the coast driven by the  
 122 tectonic context in the area (Hill and Exon, 2004), resulted in a progressive change from  
 123 dominance of shallow terrigenous sediments to pelagic carbonates during the Middle Oligocene  
 124 (Exon et al., 2001). Therefore, the continuous stratigraphic sequence at Site ODP 1168 evolves

125 from shallow-marine silty claystone in the latest Eocene and Early Oligocene, to clay-rich chalk  
126 and nannofossil ooze in the Miocene (Exon et al., 2001).

127 The paleoceanographic context is also paced by the progressive deepening of the Tasmanian  
128 Gateway, which played an important role in paleocirculation changes. The initial exchange of  
129 marine waters through the Gateway started during the Eocene (Stickley et al., 2004b). By 30 to  
130 29 Ma, neodymium isotopes from fish teeth (recording bottomwater chemistry) at Site 1168  
131 and the nearby but deeper Site 1172 had descended from typical Pacific signatures to values  
132 identical to the the Indian and Atlantic endmember, indicative of eastward flowing deep current  
133 from the Indian into the Pacific through an open gateway, inferred to indicate the onset of the  
134 Antarctic Circumpolar Current (ACC) (Scher et al., 2015).

135 For this study, 81 samples have been selected from Site 1168 Hole A in the 720 to 274 mbsf  
136 section of the recovered sequence. During our interval of focus, sediments are characterized by  
137 a gradual increase in %CaCO<sub>3</sub> content, from 10 % up to 70 %; particle size is dominantly silt  
138 and clay with sand content below 20 %, and Total Organic Carbon (TOC%) below 2% (Exon  
139 et al., 2001). This contrasts with older deposits, which feature higher TOC, larger grain size and  
140 lower carbonate content typical of nearshore conditions.

141 Today, Site 1168 is located north of the Polar Front (PF), Subtropical Front (STF) and the  
142 northern boundary of the ACC. Nevertheless, the site location has drifted in latitude following  
143 the Australian plate spread to the north away from Antarctic continent. Paleogeographic models  
144 estimate 7 degrees northward shift from 30 Ma to 15 Ma (Torsvik et al., 2012) from a  
145 paleolatitude of 55°S to a latitude of around 49°S. In addition, frontal position has also evolved  
146 since the Oligocene. The reconstructed paleoposition of the PF based on microfossil  
147 assemblages of diverse cores in the area is in the range from 60°S to 66°S (Scher et al., 2015).  
148 Although several reference frames of latitude drift have been reconstructed (O'Neill et al., 2005;  
149 Torsvik et al., 2008; Torsvik et al., 2012), in all of them Site 1168 appear to transit northward  
150 out of influence of the PF around 30 Ma and in no case later than 29.5 Ma.

151 The age model for Site 1168 has been in continuous revision since the first published shipboard  
152 reference based on biostratigraphy and magnetostratigraphic reversals (Pfuhl and McCave,  
153 2003; Stickley et al., 2004a). Subsequent further refinements in nannofossil biostratigraphy  
154 provide a new detailed age model across the Oligocene to Miocene transition (Mcgonigal, 2004)  
155 which agrees well with previous chronology. In this study, we apply chronology updated to the  
156 Geological Time Scale from Gradstein et al. (2012) by Guitián et al. (2020) and modelled based  
157 on the original magnetostratigraphy and biostratigraphy (Stickley et al., 2004a) with resulting  
158 95% confident intervals within 800kyr in the Oligocene and 400ky in the Miocene. Average  
159 sampling resolution is 290kyr. Although original magnetostratigraphy from 22 Ma to 21 Ma  
160 have uncertainties related to the weak magnetic signal, and there is some disagreement with  
161 biostratigraphic points (Mcgonigal, 2004; Stickley et al., 2004a) we consider this chronology  
162 sufficiently resolved for the long term and low-resolution scale of this study.

### 163 **3. Methods**

#### 164 **3.1 Organic extraction and biomarker analysis.**

165 Preparation of organic samples was performed on a total lipid extract (TLE). From the samples  
166 selected to reach the target resolution, TLE was obtained from approximately 30g of freeze-

167 dried disaggregated sediment extracted with an Accelerated Solvent Extractor 350. Solvent  
168 CH<sub>2</sub>Cl<sub>2</sub>/MeOH (9:1 v/v) in for four static cycles was used at 100°C. Once concentrated under  
169 purified N<sub>2</sub> stream, TLE was saponified with ~2 ml of a 0.5 M KOH in 95:5 MeOH:H<sub>2</sub>O  
170 (optima grade). The neutral fraction was obtained using 0.5ml of Hexane shaking and pipetting  
171 out the saponified fraction three times. Silica gel column chromatography was then applied for  
172 further purification by eluting 4ml of Hexane, 4ml of CH<sub>2</sub>Cl<sub>2</sub> and 4ml of MeOH for separation  
173 of the neutral fraction into a hydrocarbon fraction, a ketone fraction, including the long chain  
174 alkenones (LCA) and a polar fraction respectively.

175 Additional sample resolution was obtained from samples extracted at Utrecht University by  
176 Milestone Ethos X microwave system. CH<sub>2</sub>Cl<sub>2</sub>:MeOH 1:1 v/v was added to powdered and  
177 freeze-dried sample. This set of samples was not saponified, but only purified by column  
178 chromatography straight after the extraction splitting the TLE into an apolar, ketone and polar  
179 fraction using Hexane: CH<sub>2</sub>Cl<sub>2</sub> (9:1 v/v), Hexane: CH<sub>2</sub>Cl<sub>2</sub> (1:1 v/v) and CH<sub>2</sub>Cl<sub>2</sub>:MeOH (1:1  
180 v/v).

181 Quantification of alkenones was performed by a Thermo Scientific Trace 1310 Gas  
182 Chromatograph (GC) equipped with a Flame Ionization Detector (FID) at ETH Zurich. The GC  
183 column was an Agilent VF – 200ms (60 m X 0.25 mm X 0.25 mm) coupled to a 5-m guard  
184 column from where 4 to 5 cm were trimmed before every sequence to avoid condensation or  
185 stack of non-eluting compounds. Helium at 2-ml/min was used as carrier gas flow. The GC  
186 oven was set at 60°C for one minute after injection and then ramped at 20°C/min to 255°C,  
187 3°C/min to 300°C and finally 10°C/min to 320°C to be held 5 min. Several replicates and  
188 injection of an in-house alkenone standard (provided by G. O'Neil (Western Washington  
189 University) and C. M. Reddy (Woods Hole Oceanographic Institution) as well as n-alkane  
190 standards at every sequence were used to monitor the precision of the measurement and the  
191 performance of the instrument yielded a precision of 0.012  $U_{37}^{k'}$  units.

### 192 **3.2 Alkenone unsaturation indices and Sea Surface Temperature estimations**

193 We used the distribution and abundance of present long chain alkenones (LCA) biosynthesised  
194 by the haptophyte marine algae coccolithophores, to estimate previously defined carbon  
195 unsaturation indices. For temperature estimations, we applied the commonly used in  
196 palaeoceanography  $U_{37}^{k'}$  ratio (Brassell et al., 1986; Prahl and Wakeham, 1987), based on the  
197 relative abundances of two compounds, C<sub>37:2</sub> and C<sub>37:3</sub>, each with 37 carbon atoms and two or  
198 three carbon double bonds respectively:

$$199 \quad U_{37}^{k'} = \frac{C_{37.2} \text{ Me}}{(C_{37.2} \text{ Me} + C_{37.3} \text{ Me})}$$

200 The 37-carbon methyl ketones, possess more double bonds with colder water temperatures.  
201 Alkenone-derived SST record was estimated based on the  $U_{37}^{k'}$  unsaturation index using the  
202 BAYSPLINE calibration from Tierney and Tingley (2018). Although for high  $U_{37}^{k'}$  in the  
203 BAYSPLINE calibration, uncertainties become larger, this calculation has the advantage of  
204 propagating the error through the SST calculations since errors are not uniform across the entire  
205 temperature range.

206 The  $U_{37}^{k'}$  temperature calibrated with recent sediment samples and tested with culture studies  
207 for modern LCAs strains is widely assumed to yield accurate temperatures for earlier times in  
208 the Cenozoic. However, it has been proposed that non-thermal factors such as haptophyte algae  
209 assemblage composition or surface ocean productivity could affect the long chain alkenone  
210 distribution and abundances and therefore could bias the initial alkenone-derived SST  
211 reconstruction (Conte et al., 1998; Prahl et al., 2006) since  $U_{37}^{k'}$  is calibrated to specific  
212 environment strains. Particularly for marginal ocean environments, it is proposed that  
213 environments with strongly contrasting salinity may host different alkenone-producing strains  
214 (Kaiser et al., 2017; Longo et al., 2016).

215 The analytical instrumentation applied in this study (mid-polarity stationary phase column, VF-  
216 200ms) identifies both C<sub>37</sub> and C<sub>38</sub> methyl and ethyl long chain alkenones with good resolution  
217 in the chromatogram (Longo et al., 2013). Therefore, when the C<sub>38</sub> had sufficient concentration  
218 in our samples and were well resolved, we report  $U_{38Me}^{k'}$  (Conte and Eglinton, 1993) derived  
219 from the distribution of the C<sub>38</sub> methyl substitution:

$$220 \quad U_{38Me}^{k'} = \frac{C_{38.2} \text{ Me}}{(C_{38.2} \text{ Me} + C_{38.3} \text{ Me})}$$

221 The index  $U_{38Me}^{k'}$  has been previously suggested to be a more robust indicator of temperatures  
222 in settings which may be inhabited by diverse communities of haptophytes (Zheng et al., 2019)  
223 including members of Group II and Group I phylogenies as well as the typical marine Group  
224 III alkenone producers following the phylogenetic naming convention of Theroux et al. (2010).  
225 Today such mixtures of communities are most common in coastal or estuarine environments.  
226 These communities appear to have diverse intercepts between  $U_{37}^{k'}$  and temperature (D'Andrea  
227 et al., 2016), potentially confounding paleotemperature estimates if the community composition  
228 is varying or is not represented by the same community as the calibration equation. In such  
229 settings the index  $U_{38Me}^{k'}$  is expected to be more reliable because while C<sub>37</sub> alkenones may be  
230 produced by Group I, II, and III, the relative production of methyl C<sub>38</sub> is much greater in Group  
231 III marine alkenone producers, making its source and calibration therefore more restricted  
232 (Zheng et al., 2019).

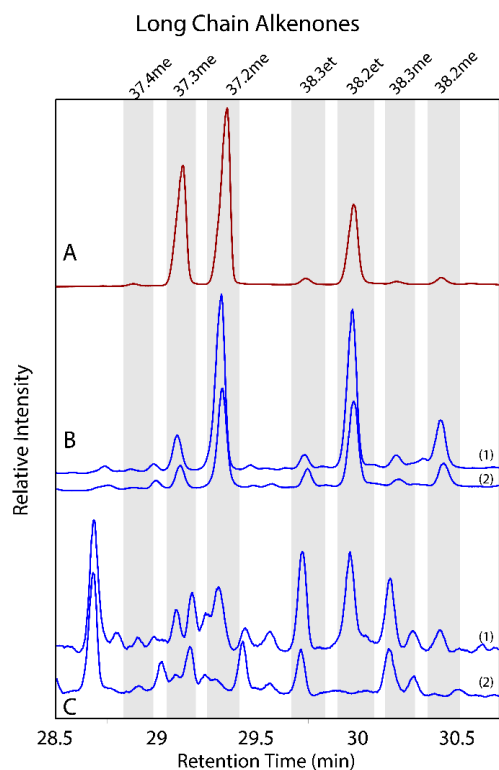
233 To additionally explore potential algae distribution influencing the SST reconstruction, we  
234 computed further indices between C<sub>37</sub> and C<sub>38</sub> alkenones, since sensitivity of them to  
235 temperature is variable depending of the saline environment (Zheng et al., 2019). The ratio  
236 between them C<sub>37</sub>/C<sub>38</sub> (Rosell-Melé et al., 1994); relationship between all C<sub>37</sub> and the ethyl C<sub>38</sub>  
237 alkenones C<sub>37</sub>/C<sub>38</sub>Et; the ratio between the methyl and ethyl C<sub>38</sub> alkenones C<sub>38</sub>Me/C<sub>38</sub>Et, and  
238 the specific compound RK2 ratio between di-unsaturated C<sub>37</sub> methyl and C<sub>38</sub> ethyl alkenones  
239 (RK2=C<sub>37.2</sub>Me/C<sub>38.2</sub>Et) (Zheng et al., 2019).

## 240 **4. Results**

### 241 **4.1 Long Chain Alkenones abundance and distribution**

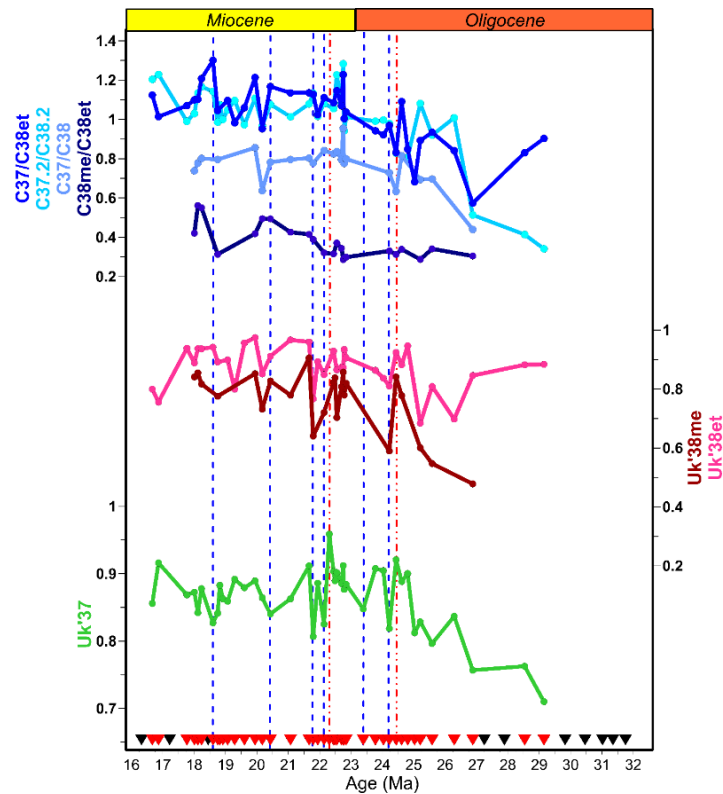
242 The total of 53 samples extracted at ETH Zurich had diverse distribution of organic compound  
243 in the ketone fraction examined (Figure 2). The subset of samples which were not saponified  
244 but only purified with column chromatography present, as expected, a greater diversity of

245 organic compounds, however the samples younger than 25 Ma, and some prior to 25 Ma, had  
246 well resolved and quantifiable LCA (Figure S1).



247  
248 **Figure 2.** Illustrative chromatograms and long chain alkenones peaks of Site 1168 samples. (a)  
249 In-house alkenone standard. (b) Examples of well-resolved alkenones samples (1= 1168A-41X-  
250 4 W, 57.0-61.0 cm 22.1 Ma; 2= 1168A-37X-4 W, 52.0-58.0 cm 20.4 Ma). (c) Sample examples  
251 of unresolved chromatogram (1= 1168A-61X-1 W, 45.0-51.0 cm 27.9 Ma; 2= 1168A-75X-4  
252 W, 130.0-136.0 cm 31 Ma).

253 With the methodology applied in this study, most of the samples older than 25.5 Ma present  
254 unresolved chromatograms in the retention time range corresponding to LCAs (Figure 3, Figure  
255 S1). These coeluting compounds complicate and in many cases preclude identification and  
256 quantification of chromatogram peak area. Only 8 samples in this segment featured  
257 chromatograms clean enough to quantify the various alkenones with confidence, including 3  
258 where saponification was not performed.



259

260 **Figure 3.** Biomarker results from ODP Site 1168. Vertical dashed lines after 25.5 Ma highlight  
 261 lower and higher  $U_{37}^{k'}$  than the mean variation with blue and red colours respectively. Bottom  
 262 black and red triangles show samples with respectively unresolved and well resolved  $C_{37.3}$  and  
 263  $C_{37.2}$  compounds.

264 In contrast, the interval younger than 27 Ma is characterized by well resolved and identified  
 265 long chain alkenones. In the ketone fraction, most of the  $C_{37}$  and  $C_{38}$  LCAs feature peaks with  
 266 good shape and no coelution. From the chromatograms of this set of clean samples we are able  
 267 to identify always two of the  $C_{37}$  ketones, the less abundant tri- and more abundant di-  
 268 unsaturated alkenones. The  $C_{38}$  ketones, when all are present and resolved, have similar  
 269 concentrations as the  $C_{37}$  being the  $C_{38.2}$  ethyl ketone the most abundant. Some samples  
 270 additionally presented  $C_{39}$  ethyl alkenones, however these were always below the detection  
 271 limit for the analysis attempted in this study.

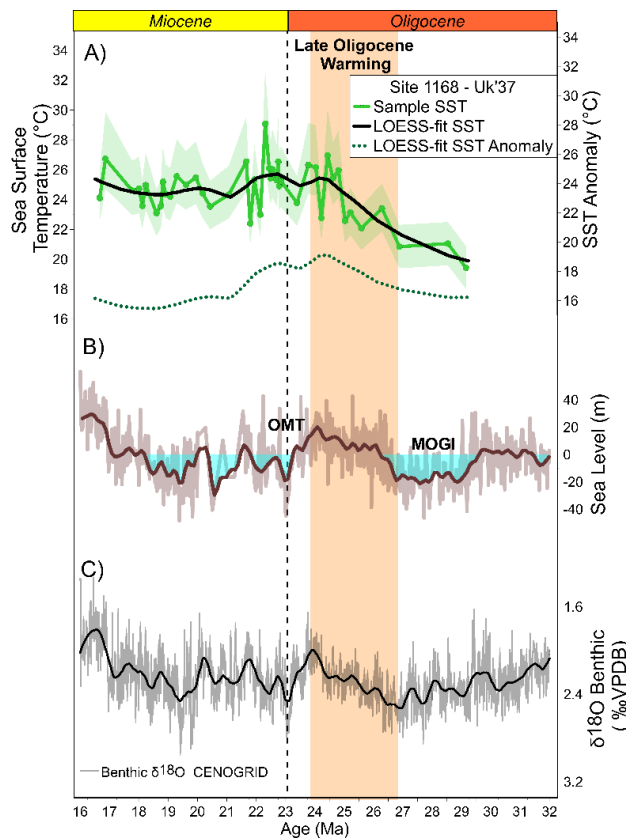
272 The ratio between all  $C_{37}$  and  $C_{38}$  alkenones gradually increases from 0.4 at 26.8 Ma to 0.9-1  
 273 by the Miocene (Figure 3). The compound specific ratio  $C_{37.2}/C_{38.2}$  also gradually increases  
 274 from 0.3 in the first identified sample at 29.2 Ma to 1.2 by the end of the record in the Miocene.  
 275 The  $C_{37}/C_{38Et}$  ratio follows a similar trend and values as the total  $C_{37}/C_{38}$  and  $C_{37.2}/C_{38.2}$ , with  
 276 the exception of the two oldest samples, which feature high ratios of  $C_{37}/C_{38Et}$ .

277 For the studied time interval,  $U_{37}^{k'}$  ratio is presented and discussed for 43 samples from the most  
 278 purified set, while the  $C_{38}$  unsaturation index  $U_{38Me}^{k'}$  is resolved only in 24 samples. The oldest  
 279 samples measured, at 29.2 Ma, feature the lowest  $U_{37}^{k'}$  of 0.7. Subsequently  $U_{37}^{k'}$  rises to 0.95 at  
 280 22.3 Ma, before stabilizing around 0.88 in the Early Miocene. The Index  $U_{38Me}^{k'}$  follows a  
 281 similar pattern despite the lower resolution. The highest correlation with  $U_{37}^{k'}$  is found in the  
 282  $U_{38Me}^{k'}$  index ( $r^2=0.82$ ) followed by the specific compound ratio  $C_{37.2}/C_{38.2Et}$  ( $r^2=0.6$ ) (Figure

283 S2). No relationship is found between obtained temperature related indices,  $U_{37}^{kl}$  and  $U_{38Me}^{kl}$ , and  
 284 the broad estimated concentration estimations of alkenone C<sub>37</sub> and C<sub>38</sub> applied in this work  
 285 (Figure S2, S3).

#### 286 4.2 Late Oligocene to Early Miocene SST estimations

287 BAYSPLINE-derived SST using the  $U_{37}^{kl}$  index range from 19°C to 29°C in the Late Oligocene  
 288 to Early Miocene at ODP Site 1168 (Figure 4). Data show long-term warming in the Late  
 289 Oligocene of 5°C, from 29 Ma (~21°C) to 24.7 Ma (~26°C) coincident with the Late Oligocene  
 290 Warming originally identified in benthic isotope records (Pälike et al., 2006; Pekar et al., 2006).  
 291 Average temperatures are stable around 25°C through the Oligocene to Miocene transition to  
 292 later cool down 2°C into the Miocene from 22.6 to 21.1 Ma. Later on, stable temperatures,  
 293 around 24.5°C characterize the record.



294

295 **Figure 4.** SST reconstruction for ODP Site 1168 and global climatic signatures. (a) Mean SST  
 296 Bayspline reconstruction with 1-sigma CI (green). Black line describe fitted data with LOESS  
 297 model. Dashed line shows SST anomaly reconstruction. (b) Sea level reconstructions from  
 298 Miller et al. (2020). Filled blue colour are intervals with negative sea level. (c) Benthic  
 299 foraminifer oxygen isotope reference (Westerhold et al., 2020). Vertical orange band shows the  
 300 interval identified as the Late Oligocene Warming.

## 301 5. Discussion

### 302 5.1 Confirmation of marine-dominated SST signal with LCA

303 Because the environment of sediment deposition at ODP 1168 went through significant changes  
 304 over the 12 million year interval explored here, before interpreting the SST signal we assess the  
 305 potential effect of changing sedimentary environment on the biomarker signal. Furthermore,

306 while alkenone SST is a widely applied proxy and a marine core top calibration is widely  
307 established (Conte et al., 2006; Müller et al., 1998; Tierney and Tingley, 2018), recent studies  
308 have revealed that diverse phylogenetic lineages characterize alkenone production in  
309 freshwater, brackish, and marine environments (Theroux et al., 2010). Contrasting lipid  
310 distributions in these lineages may contribute to varying  $U_{37}^{k'}$  index at the same temperature  
311 among the different lineages (D'Andrea et al., 2016). Today, some marine environments allow  
312 the coincidence of both open ocean alkenone producers and the Group II alkenone producers  
313 typical in estuarine environments (Longo et al., 2013; Zheng et al., 2019). Because ODP 1168  
314 was located near the coast in the early Oligocene, we therefore use a wide array of lipid indices  
315 to evaluate whether that the  $U_{37}^{k'}$  index and marine calibration are yielding appropriate  
316 temperature estimates.

317 The lowermost sediments analyzed here are characterized by a greater diversity and complexity  
318 of biomarkers and coincide with the high TOC % (>1%wt) and low  $\text{CaCO}_3$  (<10%)  
319 characteristic of the marginal and deltaic marine settings in the Early Oligocene at the location  
320 (Exon et al. (2001); Figure S1). The diversity of organic compounds might be affected by  
321 changes in diagenetic reactions as the site gradually subsides into deeper, more oxygenated  
322 waters, potentially moving out of the oxygen minimum zone by 29 Ma (Exon et al., 2001; Hill  
323 and Exon, 2004; Hochmuth et al., 2020). The good LCAs signal afterwards appear to be related  
324 to the simultaneous gradual opening of the restricted basin leading to an increase in ventilation  
325 and oxygenation of the regional water column following the invigoration of currents through  
326 the opening gateway. If sediments were subject to different oxygen exposure time, this could  
327 affect temperature estimates if more unsaturated compounds were easier to degrade as initially  
328 proposed (Brassell, 1993; Rechka and Maxwell, 1988). However, other results show less  
329 conclusive selectivity of degradation (i.e. Gong and Hollander, 1999; Grimalt et al., 2000) and  
330 affirm there is no consistent evidence of selective degradation of diunsaturated versus tri-  
331 unsaturated alkenones at depleted oxygen waters or sediments not affecting the ratio between  
332  $\text{C}_{37}$  alkenones in sediments nor while settling in the water column (Grimalt et al., 2000). Thus  
333 we conclude that the temperature estimation is not biased by evolution in the sedimentary  
334 conditions at the site.

335 Several lines of evidence suggest that SST evolution inferred from our  $U_{37}^{k'}$  is not significantly  
336 altered by changes in the contribution of non-marine alkenone producers. The main  
337 coccolithophore skeleton preserved at Site 1168 sediments are the reticulofenestrads group  
338 (Gutián et al., 2020; Wei et al., 2003). They are known to be the ancestors of the modern open  
339 ocean alkenone producers, *E. huxleyi* and *G. oceanica*, (Marlowe et al., 1990; Volkman et al.,  
340 1980; Young, 1998) included in Group III (Theroux et al., 2010) and therefore SST is  
341 interpreted from modern core top calibrations. However, the modern estuarine Group II  
342 alkenone-producers do not make mineralized skeletons so lipid indicators must be used to  
343 assess their potential contribution. Since algae from brackish to saline environments generally  
344 do not generate as  $\text{C}_{38}$  methyl alkenones as the ocean water ones (Lopez et al., 2005; Zheng et  
345 al., 2019; Zheng et al., 2017), Zheng et al. (2019) suggested that temperature reconstructions  
346 from the ratio  $U_{38Me}^{k'}$  will provide robust estimations which are free from artefacts of changing  
347 relative abundance of Group II and Group III haptophytes algae. We present unsaturation  
348 indices from the  $\text{C}_{38}$  LCAs (Figure 3; Figure S1), however,  $U_{38Me}^{k'}$  could be calculated for only

349 24 samples. We document that when large changes in  $U_{37}^{k'}$  are found, (i.e. from 29 to 24  
350 Ma),  $U_{38Me}^{k'}$  covary with  $U_{37}^{k'}$ , ( $r^2=0.82$ ). This supports interpretation of the  $U_{37}^{k'}$  as caused by  
351 SST variations, not changes in the alkenone-producing community.

352 One additional evidence of the marine origin of the  $U_{37}^{k'}$  involved lipids is the covariance  
353 obtained from the  $C_{37.2}Me$  and  $C_{38.2}Et$  relationship, RK2 index (Zheng et al., 2019) (Figure 3).  
354 Both LCAs are produced among different species groups but their ratio is more sensitive to  
355 temperature in the open marine environments strains (Zheng et al., 2019). In our dataset, the  
356 RK2 is positively correlated with the temperature related indices, which suggests the open water  
357 marine, rather than estuarine, source of LCAs ( $r^2: 0.64 U_{37}^{k'}$ ;  $r^2=0.51 U_{38Me}^{k'}$ ) (Figure S2). This  
358 evidence leads us to interpret the long-term trend in  $U_{37}^{k'}$  as most likely derived from ocean  
359 water algae assemblage and the temperature estimates are not biased due to influence of other  
360 alkenone producing families such as those found in modern coastal or low saline environments.

361 Due to the shallow position of ODP Site 1168, sedimentation likely support little horizontal  
362 drift of the organic compounds as settling down from the surface. As the surface paleo  
363 circulation followed the west-east direction with the Proto – Leeuwin current, parallel to the  
364 Australian Margin (Stickley et al., 2004b), suggests that low potential for compounds to have  
365 been produced in areas with large differences in temperatures.

366

## 367 **5.2 Site 1168 Sea Surface Temperature Trends**

### 368 5.2.1 Sensitivity of temperature trends to latitudinal movement and setting

369 Aliasing of high frequency orbital variability in SST, as well as the latitudinal movement of the  
370 site, may affect the long-term temperature trends observed at this site. To reduce the influence  
371 of high frequency variability on long-term SST variation, we also present a smooth of the long-  
372 term trend by applying a local polynomial regression model (LOESS) (Figure 4). The smoothed  
373 trend shows a long term warming of 5°C from the Middle to the Late Oligocene, reaches a  
374 maximum around 26°C during the transition from the Oligocene to the Miocene, and then cools  
375 down to stabilize at 24.5°C until the end of the record at 16.7 Ma.

376 Since the South Tasmanian margin has drifted northwards from paleolatitude of 55°S to 48°S  
377 over the Oligocene to Miocene interval sampled here, we follow the approach described by  
378 Herbert et al. (2016) to distinguish the component of SST change due to regional climate  
379 variation, from that due to the migration of the site to warmer latitudes. We calculate a  
380 temperature anomaly as the difference between the smoothed LOESS-fit temperatures for ODP  
381 Site 1168 (Figure 4) and the modern mean annual temperature (Locarnini et al., 2013) at the  
382 backtracked paleolatitude and longitude of Site 1168 position at the age of each  $U_{37}^{k'}$  sample.  
383 Paleogeography is reconstructed according to (van Hinsbergen et al., 2015) which is based on  
384 the paleo magnetic reference frame of (Torsvik et al., 2012). The estimated anomaly reaffirms  
385 that there is a regional warming in the Late Oligocene by 4°, which is not an artefact of the  
386 migration of the site. The calculated anomaly also indicates a relatively colder Early Miocene.  
387 Because the paleolatitude range of Site 1168 spans the modern Polar Front (PF) region of  
388 steepened temperature gradients, whereas the micropaleontological assemblages at multiple  
389 sites indicate that the PF remained poleward of Site 1168 in the Oligocene-Miocene (Scher et

390 al., 2015), the corrected temperature anomaly may underestimate the actual regional warming  
391 through the Oligocene to Early Miocene.

392 We propose that the SST trends obtained from Site 1168 between 29.2 Ma and 16.7 Ma are  
393 representative of regional warming/cooling because they postdate the reorganization of ocean  
394 currents accompanying basin opening and the northward shift of the Tasmanian margin  
395 (Stickley et al., 2004b). Neodymium isotopes on fossil fish teeth at Site 1168 confirm the  
396 eastward flow from the Pacific Ocean in intermediate depths following the northward migration  
397 of the gateway into the influence of the westerly wind achieved by 29 Ma (Scher et al., 2015).  
398 Paleobathymetry reconstructions further support the existence of an important shallow to  
399 intermediate water exchange already by 30 Ma (Hochmuth et al., 2020).

#### 400 5.2.2 Late Oligocene – Early Miocene SST trends

401 Our Southern Hemisphere SST record commences a few million years after the abrupt decrease  
402 in deep ocean temperature and increase in Antarctic ice volume recorded by benthic  $\delta^{18}\text{O}$  across  
403 the EOT (Figure 4). Our record begins within the MOGI, defined by oxygen isotope records  
404 and a 2-myrr lowstand sea level (Liebrand et al., 2017; Miller et al., 2020), and we record  
405 relatively low SST. The most prominent feature of our SST record is the warming of up to  
406  $5.5^\circ\text{C}$  in the LOESS-smoothed record represented by  $4^\circ\text{C}$  increase in the calculated SST  
407 anomaly, from ca 29 to 24.5 Ma. This long term warming is simultaneous, within the age  
408 uncertainty, with the negative long term benthic  $\delta^{18}\text{O}$  shift starting at 27 Ma (De Vleeschouwer  
409 et al., 2017; Zachos et al., 2008) described as the Late Oligocene Warming (Pekar et al., 2006;  
410 Villa and Persico, 2006).

411 The transient cooling and ice build-up reflected in a large positive benthic excursion at the  
412 Oligocene Miocene boundary was likely not sampled by the resolution of this study. Light  
413 reflectivity ( $L^*$ ) generated by the shipboard expedition (Exon et al., 2001), does present a  
414 significant turning point at the surrounding depths of the expected OMT applying the age model  
415 from Guitián et al. (2020) used in this study (Figure S4), coincident with changes in rates of  
416 sediment accumulation, where SST is not sampled. These data suggest that our smoothed trends  
417 over the Oligocene Miocene transition do omit orbital events of shorter duration..

418  
419 Our estimates of temperature anomaly suggest an average colder Early Miocene than latest  
420 Oligocene, with a 1-myrr. cooling from  $25.5^\circ\text{C}$  starting at 22.7 Ma, to stabilization of absolute  
421 temperatures around  $24.4^\circ\text{C}$  thereafter until 16.7 Ma (Figure 4). Those estimates are in  
422 agreement with relatively lower sea level reconstructions in the Early Miocene, and more  
423 positive benthic  $\delta^{18}\text{O}$ , although benthic records feature higher variability than Miocene SSTs at  
424 ODP 1168.

425 During the Early Oligocene, the cool SST we have reconstructed at Site 1168 are largely  
426 coherent with the available SST estimates from nearby sites in the Southern Ocean and expected  
427 post-EOT latitudinal temperature gradients (Kennedy-Asser et al., 2020) (Figure 1). In the  
428 Atlantic sector of the Southern Ocean at ODP Site 1090, with estimated paleolatitude  $7^\circ$   
429 equatorward of Site 1168, average alkenone-derived temperatures are  $3.1^\circ\text{C}$  warmer than Site  
430 1168 in the Early Oligocene (27.7 to 33 Ma)(Liu et al., 2009), in agreement with the modelled  
431 latitudinal gradient for post EOT times (Kennedy-Asser et al., 2020). The average  $2.3^\circ\text{C}$   
432 warmer GDGTs-derived temperatures at nearby Site 1172 at 30 Ma (Houben et al., 2019) could

433 reflect a greater influence of warm poleward currents at ODP 1172 or effects of different proxy  
434 calibration or habitat (Figure 1; Table S1). Compared to temperatures estimated at a pre-EOT  
435 33 Ma time slice east of the Tasmanian Gateway at DSDP 277 (Liu et al., 2009), our oldest  
436 temperature estimates are only 3.1°C and 4.7°C colder than alkenone and GDGT-derived  
437 reconstructed temperatures, respectively. The most surprising comparison is that our early  
438 Oligocene temperatures are considerably warmer than those obtained at ODP Site 511 (31-32.5  
439 Ma), east of the Drake Passage in the South Atlantic, which estimated 9°C alkenone -derived  
440 and 15°C GDGTs-derived temperatures (Houben et al., 2019; Liu et al., 2009).

441 Our mid Miocene (16.7 Ma) estimate of 24°C SST at Site 1168 is consistent with recent TEX<sub>86</sub>  
442 reconstructions at Site 1171, located only 700 km further south east (Figure 1) that indicates  
443 mid Miocene temperatures of 26°C at 15.5 Ma (Leutert et al., 2020). Site 1168 SST are, on the  
444 other hand 5.5°C warmer than TEX<sub>86</sub> temperatures estimates found at the Antarctic Margin  
445 (Hartman et al., 2018). Our estimation of colder early Miocene temperatures are consistent with  
446 terrestrial indicators suggesting a landscape similar to the modern tundra in the continent  
447 (DSDP 270; also seen at CRP-2 Kulhanek et al. (2019)); marine records suggest and lower SST  
448 in the area and a distal ice sheet grounding-line.

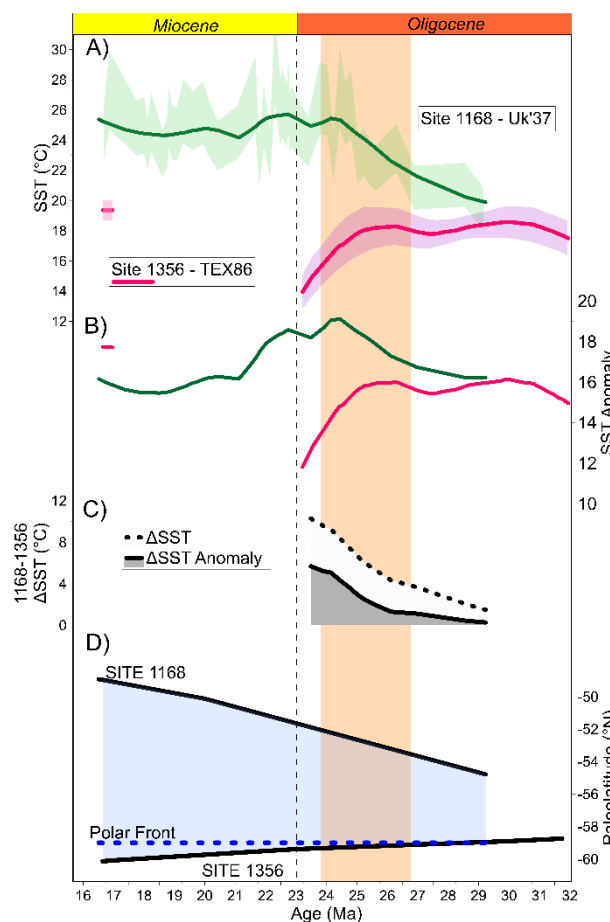
### 449 **5.3 Evolution of temperature gradients in the Southern Ocean**

450 Because in the Oligocene- - Early Miocene global ice volume was concentrated in Antarctica,  
451 and because deep-water formation is interpreted to have occurred in the Southern Ocean, the  
452 evolution of SST in the Southern Ocean is of particular relevance to interpretations of the  
453 benthic  $\delta^{18}\text{O}$  and its potential ice volume and deep ocean temperature components. It is widely  
454 assumed that ice volume is coupled to deep-water temperatures, but recent model simulations  
455 suggest that this relationship is nonlinear and that there may be very limited changes in deep-  
456 water temperature when Antarctic ice sheet height but not aerial extent varies (Bradshaw et al.,  
457 2021). If the 3°C warming of SST estimated from the Site 1168 temperature anomaly over the  
458 LOW was broadly representative of temperature trends elsewhere in the Southern Ocean,  
459 including regions of deep-water formation, this would suggest that the ~27 to 24 Ma trend in  
460 benthic  $\delta^{18}\text{O}$  marking the LOW could have a significant deep ocean temperature component.  
461 However, deep-water temperatures estimated from the Mg/Ca of benthic foraminifer in deep  
462 Pacific sites (Cramer et al., 2011; Lear et al., 2004) suggest negligible temperature change  
463 across over this time interval. If this deep-water temperature trend is not affected by  
464 uncertainties in the benthic Mg/Ca calibration and effect of secondary influences (Hollis et al.,  
465 2019), it suggests a large decrease in ice volume responsible for the benthic  $\delta^{18}\text{O}$  shift over the  
466 LOW.

467 If bottom water temperatures did not change through the LOW, then the warming at Site 1168  
468 suggests an increasing latitudinal temperature gradient between the Antarctic margin site of  
469 deep-water formation and the Tasmanian Rise. Indeed GDGTs-derived SST on the Wilkes Land  
470 Antarctic Margin Site 1356 over this interval (consistently at 60°S, Figure 1 Map (Torsvik et  
471 al., 2012; van Hinsbergen et al., 2015)) also show no evidence of warming through the Late  
472 Oligocene (Hartman et al., 2018; Salabarnada et al., 2018) (Figure 5). If TEX<sub>86</sub> at Wilkes land  
473 margin accurately records changes in SST during this time period without bias from reworking  
474 (Bijl et al., 2018; Hartman et al., 2018; Hoem et al., 2020) the data imply an increasing thermal  
475 gradient between Site 1168 and the Wilkes land margin (Figure 5). Potentially, the final opening

476 of the Tasmanian Gateway by 27.5 Ma caused in the alignment of the westerlies winds with the  
 477 Drake passage and a gradual strengthening of the proto-ACC (Exon et al., 2001; Nicholson and  
 478 Stow, 2019; Pfuhl and McCave, 2005; Pfuhl et al., 2004; Scher et al., 2015) reducing the  
 479 poleward heat transport towards the Wilkes Land Antarctic margin. However, this  
 480 interpretation of increasing thermal isolation of Antarctica resulting in constant deepwater  
 481 temperatures would then require additional mechanisms other than proximal ocean warmth to  
 482 trigger the hypothesized decrease in Antarctic ice volume during the LOW. Furthermore, the  
 483 absence of deep-water temperature change would imply the LOW was characterized by  
 484 primarily by a reduction in Antarctic ice sheet height. In the absence of proximal ocean  
 485 warming, one mechanism to trigger ice retreat might be greenhouse forcing, however  $\epsilon_p$ -based  
 486 proxy long term estimates suggest decreasing or stable  $\text{CO}_2$  through the LOW (Zhang et al.,  
 487 2013).

488 Alternatively, GDGT-based SST estimates in the North Atlantic do not resolve warming trends  
 489 that are resolved by alkenone-based SST (Gutián et al., 2019). If this is true on the Wilkes  
 490 margin, then the potential for broad Southern Ocean warming may need to be further explored.  
 491 Given uncertainties in both deep-water and SST proxies, additional temperature records at  
 492 different latitudes in the Southern Ocean at this time would be useful to distinguish the spatial  
 493 extent of Southern Ocean warming during the LOW and the nature and cause of any ice volume  
 494 changes at this time.



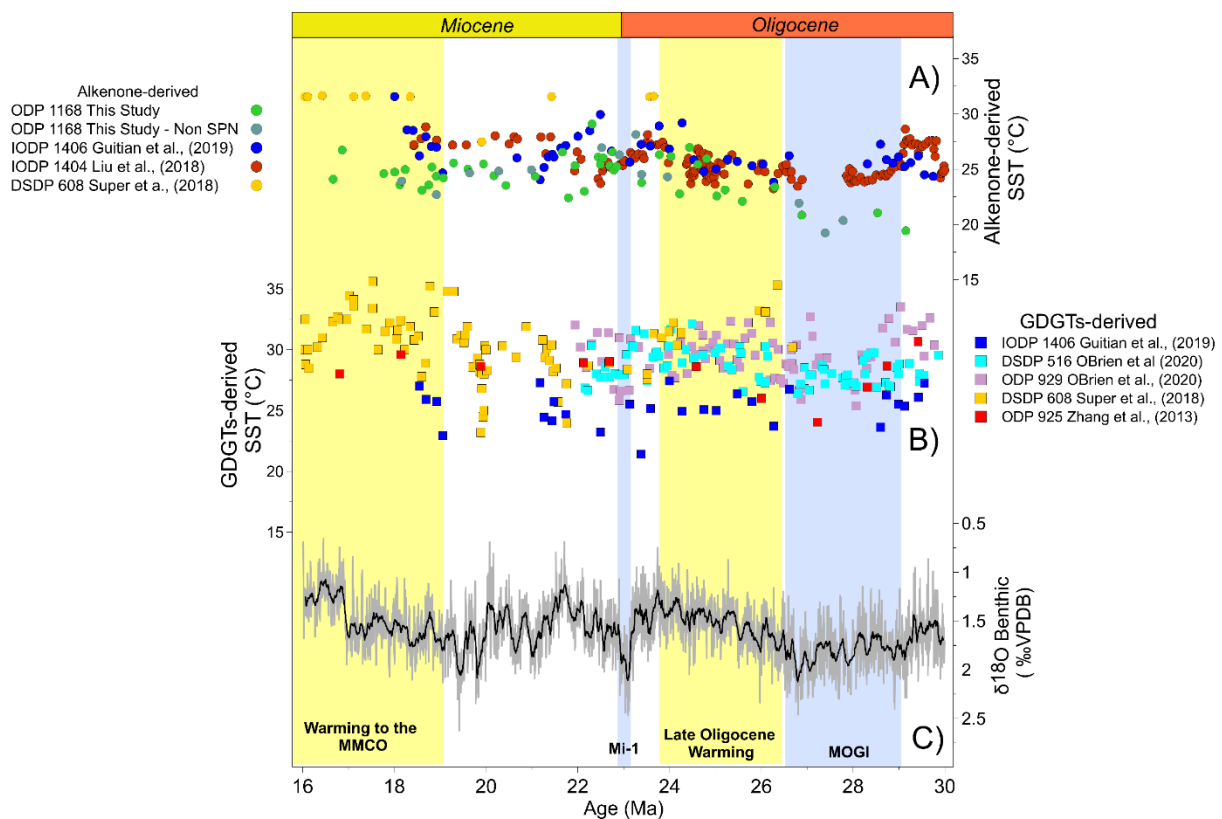
495

496 **Figure 5.** (a) SST reconstructions from  $U_{37}^{kl}$  ODP 1168 and  $\text{TEX}_{86}$  ODP 1356 (Hartman et al.,  
 497 2018). (b) Reconstructed SST anomaly for both sites. (c) Temperature gradient between ODP

498 1168 and ODP 1356. (d) Paleolatitude estimations for both sites ODP 1356 (Torsvik et al.,  
 499 2012; van Hinsbergen et al., 2015) and estimated position of the PF between the two sites  
 500 (Salabarnada et al., 2018; Scher et al., 2015) using same paleolatitude reconstruction frame.

#### 501 5.4 Late Oligocene Warming magnitude in the Southern and Northern Hemisphere

502 Although there are hiatuses during the MOGI in mid-latitude Northern hemisphere sites,  
 503 alkenone-derived SST suggest similar magnitude warming as Site 1168 (Figure 6). Our  
 504 Southern Ocean inference of 4°C of SST-anomaly from 29 Ma to the stabilization at 24.5 Ma  
 505 is similar to ca 3°C warmer Late Oligocene than the preceding Early Oligocene inferred from  
 506 alkenone-derived temperatures from 40°N Atlantic Site 1406 (Gutián et al., 2019). Likewise,  
 507 at nearby IODP Site 1404 SST increases by 4°C from 26.8 to 23.5 Ma. a (Liu et al., 2018).



508  
 509 **Figure 6.** Oligocene to Miocene long-term SST records from low to mid latitude sites classified  
 510 by proxy. (a) Alkenone-derived SST calibrated from the  $U_{37}^{kr}$  ratio with BAYSPLINE (Tierney  
 511 and Tingley, 2018). (b) GDGTs-derived SST from  $TEX_{86}$  using BAYSPARE calibration  
 512 (Tierney and Tingley, 2015). Note that SST records are presented without adjustment for  
 513 latitudinal shift at any site as it is likely that only Site 1168 present significant anomaly. Both  
 514 SST axis show equivalent magnitude. Vertical yellow and blue bands show main warming and  
 515 cold period discussed in the text. (c) Benthic reference megasplice (De Vleeschouwer et al.,  
 516 2017).

517 The LOW has been more difficult to distinguish in GDGT-derived SST estimates. Northern  
 518 Hemisphere GDGT-derived records from mid-latitude Sites DSDP 608 and IODP Site 1406,  
 519 do not support any warming across the Late Oligocene (Gutián et al., 2019; Super et al., 2018)  
 520 despite similar latitude to our Southern Hemisphere Site 1168 record. Only southern mid-  
 521 latitude Atlantic Site 516 GDGTs-reconstructions identify a clear increase of the mean

522 temperature coincident with Site 1168 alkenone-derived SST from 27.5 to 24 Ma, but this is a  
523 modest change of only 1.5°C and no lower temperature sampled earlier in the middle Oligocene  
524 (O'Brien et al., 2020). High resolution (100ky) GDGTs reconstructions at Equatorial Atlantic  
525 ODP Site 929 show no evident warming over the entire Late Oligocene –Miocene, and if there  
526 is one, appear to be only 2.5°C from 26.5 Ma to 25.5 Ma (O'Brien et al., 2020). Because the  
527  $U_{37}^{K'}$  ratio is saturated in most tropical sites, estimations of polar amplification at the moment  
528 rely on comparison of low latitude GDGT-based SST records with the higher latitude alkenone-  
529 based records, potentially conflating proxy-specific effects with true variations in the latitudinal  
530 expression of the Late Oligocene climate changes.

## 531 **6. Conclusions**

532 The Tasmanian Sea ODP Site 1168 alkenone-derived SST record shows for the first time cold  
533 conditions related with the MOGI, and confirms in the Southern Hemisphere, the previously  
534 recognized subsequent long-term warming through the Late Oligocene. By 29 Ma, 20°C, SST  
535 characterized the middle Oligocene at Site 1168. A subsequent 5°C increase in SST between  
536 27 and 24.5 Ma coincided with the end the MOGI. Apparent warmer temperatures exist during  
537 the latest Oligocene and transition to the Miocene around 24.5-22.5°C, cooling down 2°C to  
538 finally stabilize into the Miocene around 20.1 Ma, although the Oligocene Miocene transition  
539 might not be sampled here. The variability of SST is higher in the warm Late Oligocene and  
540 more stable in the relatively colder Early Miocene. Reconstructed latitudinal drift of the site  
541 does not explain the observed long-term temperature trends. Calculated true temperature  
542 anomalies for a given latitude still document a significant late Oligocene SST increase.  
543 Comparison with previously published records from the Atlantic Ocean and surrounding  
544 Antarctic locations, highlights the discrepancy in warming amplitude among records from  
545 differing proxies and locations and underscores the need for further evaluation of proxies and  
546 oceanic circulation to provide a coherent picture of Southern Ocean climate evolution through  
547 the Oligocene to early Miocene.

## 548 **7. Acknowledgments and Data**

549 Sediment samples were provided by the Ocean Drilling Program (ODP). This study was  
550 supported by the Swiss National Science Foundation (Award 200021\_182070 to Heather Stoll).  
551 Authors are very thankful to Madalina Jaggi, Stewart Bishop, and Thierry Solms for assistance  
552 in the laboratory. We also thank Lena Thöle and Mariska Hoorweg for providing the subset of  
553 samples from Utrecht University with an ERC starting grant n802835 OceaNice to Peter K.  
554 Bijl. Data generated for this work is uploaded as independent excel file as Supplementary  
555 Information Table S2 and archived online at Zenodo Data Archive (link will be provided once  
556 manuscript is accepted).

## 557 **8. References**

558 Bijl, P.K., Houben, A.J., Hartman, J.D., Pross, J., Salabarnada, A., Escutia, C., Sangiorgi, F.,  
559 2018. Paleooceanography and ice sheet variability offshore Wilkes Land, Antarctica-Part 2:  
560 Insights from Oligocene-Miocene dinoflagellate cyst assemblages. *Climate of the Past* 14,  
561 1015-1033.

- 562 Bradshaw, C.D., Langebroek, P.M., Lear, C.H., Lunt, D.J., Coxall, H.K., Sosdian, S.M., de  
563 Boer, A.M., 2021. Hydrological impact of Middle Miocene Antarctic ice-free areas coupled to  
564 deep ocean temperatures. *Nature Geoscience* 14, 429-436.
- 565 Brassell, S., Eglinton, G., Marlowe, I., Pflaumann, U., Sarnthein, M., 1986. Molecular  
566 stratigraphy: a new tool for climatic assessment. *Nature* 320, 129.
- 567 Brassell, S.C., 1993. Applications of biomarkers for delineating marine paleoclimatic  
568 fluctuations during the Pleistocene, *Organic Geochemistry*. Springer, pp. 699-738.
- 569 Conte, M.H., Eglinton, G., 1993. Alkenone and alkenoate distributions within the euphotic  
570 zone of the eastern North Atlantic: correlation with production temperature. *Deep Sea*  
571 *Research Part I: Oceanographic Research Papers* 40, 1935-1961.
- 572 Conte, M.H., Sicre, M.A., Rühlemann, C., Weber, J.C., Schulte, S., Schulz-Bull, D., Blanz,  
573 T., 2006. Global temperature calibration of the alkenone unsaturation index (UK' 37) in  
574 surface waters and comparison with surface sediments. *Geochemistry, Geophysics,*  
575 *Geosystems* 7.
- 576 Conte, M.H., Thompson, A., Lesley, D., Harris, R.P., 1998. Genetic and physiological  
577 influences on the alkenone/alkenoate versus growth temperature relationship in *Emiliana*  
578 *huxleyi* and *Gephyrocapsa oceanica*. *Geochimica et Cosmochimica Acta* 62, 51-68.
- 579 Cramer, B., Miller, K., Barrett, P., Wright, J., 2011. Late Cretaceous–Neogene trends in deep  
580 ocean temperature and continental ice volume: Reconciling records of benthic foraminiferal  
581 geochemistry ( $\delta^{18}\text{O}$  and Mg/Ca) with sea level history. *Journal of Geophysical Research:*  
582 *Oceans* 116.
- 583 D'Andrea, W.J., Theroux, S., Bradley, R.S., Huang, X., 2016. Does phylogeny control U37K-  
584 temperature sensitivity? Implications for lacustrine alkenone paleothermometry. *Geochimica*  
585 *et Cosmochimica Acta* 175, 168-180.
- 586 De Vleeschouwer, D., Vahlenkamp, M., Crucifix, M., Pälike, H., 2017. Alternating Southern  
587 and Northern Hemisphere climate response to astronomical forcing during the past 35 my.  
588 *Geology* 45, 375-378.
- 589 Exxon, N., Kennett, J., Malone, M., 2001. 1. LEG 189 SUMMARY, *Proceedings of the Ocean*  
590 *Drilling Program*.
- 591 Exxon, N., Kennett, J., Malone, M., Brinkhuis, H., Chaproniere, G., Ennyu, A., Fothergill, P.,  
592 Fuller, M., Grauert, M., Hill, P., 2002. Drilling reveals climatic consequences of Tasmanian  
593 Gateway opening. *Eos, Transactions American Geophysical Union* 83, 253-259.
- 594 Gong, C., Hollander, D.J., 1999. Evidence for differential degradation of alkenones under  
595 contrasting bottom water oxygen conditions: Implication for paleotemperature reconstruction.  
596 *Geochimica et Cosmochimica Acta* 63, 405-411.
- 597 Gradstein, F.M., Ogg, J.G., Schmitz, M., Ogg, G., 2012. *The geologic time scale 2012*.  
598 *elsevier*.
- 599 Grimalt, J.O., Rullkötter, J., Sicre, M.A., Summons, R., Farrington, J., Harvey, H.R., Goñi,  
600 M., Sawada, K., 2000. Modifications of the C37 alkenone and alkenoate composition in the

601 water column and sediment: Possible implications for sea surface temperature estimates in  
602 paleoceanography. *Geochemistry, Geophysics, Geosystems* 1.

603 Guitián, J., Dunkley Jones, T., Hernández-Almeida, I., Löffel, T., Stoll, H.M., 2020.  
604 Adaptations of coccolithophore size to selective pressures during the Oligocene - Early  
605 Miocene high CO<sub>2</sub> world. *Paleoceanography and Paleoclimatology* n/a, e2020PA003918.

606 Guitián, J., Phelps, S., Polissar, P.J., Ausín, B., Eglinton, T.I., Stoll, H.M., 2019. Midlatitude  
607 Temperature Variations in the Oligocene to Early Miocene. *Paleoceanography and*  
608 *Paleoclimatology* 34, 1328-1343.

609 Hartman, J.D., Sangiorgi, F., Escutia Dotti, C., 2018. Paleoceanography and ice sheet  
610 variability offshore Wilkes Land, Antarctica—Part 3: Insights from Oligocene–Miocene  
611 TEX86-based sea surface temperature reconstructions.

612 Herbert, T.D., Lawrence, K.T., Tzanova, A., Peterson, L.C., Caballero-Gill, R., Kelly, C.S.,  
613 2016. Late Miocene global cooling and the rise of modern ecosystems. *Nature Geoscience* 9,  
614 843.

615 Hill, P.J., Exon, N.F., 2004. Tectonics and basin development of the offshore Tasmanian area  
616 incorporating results from deep ocean drilling. *GMS* 151, 19-42.

617 Hochmuth, K., Gohl, K., Leitchenkov, G., Sauermilch, I., Whittaker, J.M., Uenzelmann-  
618 Neben, G., Davy, B., De Santis, L., 2020. The evolving paleobathymetry of the circum-  
619 Antarctic Southern Ocean since 34 Ma: A key to understanding past cryosphere-ocean  
620 developments. *Geochemistry, Geophysics, Geosystems* 21, e2020GC009122.

621 Hoem, F.S., Valero, L., Evangelinos, D., Escutia, C., Duncan, B., McKay, R.M., Brinkhuis,  
622 H., Sangiorgi, F., Bijl, P.K., 2020. Temperate Oligocene surface ocean conditions offshore  
623 Cape Adare, Ross Sea, Antarctica. *Climate of the Past Discussions*, 1-32.

624 Hollis, C.J., Dunkley Jones, T., Anagnostou, E., Bijl, P.K., Cramwinckel, M.J., Cui, Y.,  
625 Dickens, G.R., Edgar, K.M., Eley, Y., Evans, D., 2019. The DeepMIP contribution to PMIP4:  
626 methodologies for selection, compilation and analysis of latest Paleocene and early Eocene  
627 climate proxy data, incorporating version 0.1 of the DeepMIP database. *Geoscientific Model*  
628 *Development* 12, 3149-3206.

629 Houben, A.J., Bijl, P.K., Sluijs, A., Schouten, S., Brinkhuis, H., 2019. Late Eocene Southern  
630 Ocean cooling and invigoration of circulation preconditioned Antarctica for full-scale  
631 glaciation. *Geochemistry, Geophysics, Geosystems* 20, 2214-2234.

632 Kaiser, J., van der Meer, M.T., Arz, H.W., 2017. Long-chain alkenones in Baltic Sea surface  
633 sediments: new insights. *Organic Geochemistry* 112, 93-104.

634 Kennedy-Asser, A.T., Lunt, D.J., Valdes, P.J., Ladant, J.-B., Frieling, J., Laetano, V., 2020.  
635 Changes in the high-latitude Southern Hemisphere through the Eocene–Oligocene transition:  
636 a model–data comparison. *Climate of the Past* 16.

637 Kulhanek, D.K., Levy, R.H., Clowes, C.D., Prebble, J.G., Rodelli, D., Jovane, L., Morgans,  
638 H.E., Kraus, C., Zwingmann, H., Griffith, E.M., 2019. Revised chronostratigraphy of DSDP  
639 Site 270 and late Oligocene to early Miocene paleoecology of the Ross Sea sector of  
640 Antarctica. *Global and Planetary Change* 178, 46-64.

- 641 Lear, C.H., Rosenthal, Y., Coxall, H.K., Wilson, P., 2004. Late Eocene to early Miocene ice  
642 sheet dynamics and the global carbon cycle. *Paleoceanography* 19.
- 643 Leutert, T.J., Auderset, A., Martínez-García, A., Modestou, S., Meckler, A.N., 2020. Coupled  
644 Southern Ocean cooling and Antarctic ice sheet expansion during the middle Miocene. *Nature*  
645 *Geoscience* 13, 634-639.
- 646 Liebrand, D., de Bakker, A.T., Beddow, H.M., Wilson, P.A., Bohaty, S.M., Ruessink, G.,  
647 Palike, H., Batenburg, S.J., Hilgen, F.J., Hodell, D.A., Huck, C.E., Kroon, D., Raffi, I., Saes,  
648 M.J., van Dijk, A.E., Lourens, L.J., 2017. Evolution of the early Antarctic ice ages. *Proc Natl*  
649 *Acad Sci U S A* 114, 3867-3872.
- 650 Liu, Z., He, Y., Jiang, Y., Wang, H., Liu, W., Bohaty, S.M., Wilson, P.A., 2018. Transient  
651 temperature asymmetry between hemispheres in the Palaeogene Atlantic Ocean. *Nature*  
652 *Geoscience* 11, 656.
- 653 Liu, Z., Pagani, M., Zinniker, D., Deconto, R., Huber, M., Brinkhuis, H., Shah, S.R., Leckie,  
654 R.M., Pearson, A., 2009. Global cooling during the eocene-oligocene climate transition.  
655 *Science* 323, 1187-1190.
- 656 Locarnini, R., Mishonov, A., Antonov, J., Boyer, T., Garcia, H., Baranova, O., Zweng, M.,  
657 Paver, C., Reagan, J., Johnson, D., 2013. *World Ocean Atlas 2013, Volume 1: Temperature*,  
658 edited by: Levitus, S. A. Mishonov Technical Ed., NOAA Atlas NESDIS 73, 40.
- 659 Longo, W.M., Dillon, J.T., Tarozo, R., Salacup, J.M., Huang, Y., 2013. Unprecedented  
660 separation of long chain alkenones from gas chromatography with a poly  
661 (trifluoropropylmethylsiloxane) stationary phase. *Organic Geochemistry* 65, 94-102.
- 662 Longo, W.M., Theroux, S., Giblin, A.E., Zheng, Y., Dillon, J.T., Huang, Y., 2016.  
663 Temperature calibration and phylogenetically distinct distributions for freshwater alkenones:  
664 Evidence from northern Alaskan lakes. *Geochimica et Cosmochimica Acta* 180, 177-196.
- 665 Lopez, J.F., de Oteyza, T.G., Teixidor, P., Grimalt, J.O., 2005. Long chain alkenones in  
666 hypersaline and marine coastal microbial mats. *Organic Geochemistry* 36, 861-872.
- 667 Marlowe, I., Brassell, S., Eglinton, G., Green, J., 1990. Long-chain alkenones and alkyl  
668 alkenoates and the fossil coccolith record of marine sediments. *Chemical Geology* 88, 349-  
669 375.
- 670 Mcgonigal, K.L., 2004. Quantitative Miocene calcareous nannofossil biostratigraphy from the  
671 Tasmanian Gateway. *GMS* 151, 191-213.
- 672 Miller, K.G., Browning, J.V., Schmelz, W.J., Kopp, R.E., Mountain, G.S., Wright, J.D., 2020.  
673 Cenozoic sea-level and cryospheric evolution from deep-sea geochemical and continental  
674 margin records. *Science advances* 6, eaaz1346.
- 675 Müller, P.J., Kirst, G., Ruhland, G., Von Storch, I., Rosell-Melé, A., 1998. Calibration of the  
676 alkenone paleotemperature index U37K' based on core-tops from the eastern South Atlantic  
677 and the global ocean (60° N-60° S). *Geochimica et Cosmochimica Acta* 62, 1757-1772.
- 678 Nicholson, U., Stow, D., 2019. Erosion and deposition beneath the Subantarctic Front since  
679 the Early Oligocene. *Scientific reports* 9, 1-9.

680 O'Neill, C., Müller, D., Steinberger, B., 2005. On the uncertainties in hot spot reconstructions  
681 and the significance of moving hot spot reference frames. *Geochemistry, Geophysics,*  
682 *Geosystems* 6.

683 O'Brien, C.L., Huber, M., Thomas, E., Pagani, M., Super, J.R., Elder, L.E., Hull, P.M., 2020.  
684 The enigma of Oligocene climate and global surface temperature evolution. *Proceedings of*  
685 *the National Academy of Sciences* 117, 25302-25309.

686 Pälike, H., Norris, R.D., Herrle, J.O., Wilson, P.A., Coxall, H.K., Lear, C.H., Shackleton,  
687 N.J., Tripathi, A.K., Wade, B.S., 2006. The heartbeat of the Oligocene climate system. *science*  
688 314, 1894-1898.

689 Pekar, S.F., DeConto, R.M., 2006. High-resolution ice-volume estimates for the early  
690 Miocene: Evidence for a dynamic ice sheet in Antarctica. *Palaeogeography,*  
691 *Palaeoclimatology, Palaeoecology* 231, 101-109.

692 Pekar, S.F., DeConto, R.M., Harwood, D.M., 2006. Resolving a late Oligocene conundrum:  
693 deep-sea warming and Antarctic glaciation. *Palaeogeography, Palaeoclimatology,*  
694 *Palaeoecology* 231, 29-40.

695 Pfuhl, H.A., McCave, I.N., 2003. Integrated age models for the early Oligocene-early  
696 Miocene, sites 1168 and 1170–1172, *Proc. ODP, Sci. Results*, pp. 1-21.

697 Pfuhl, H.A., McCave, I.N., 2005. Evidence for late Oligocene establishment of the Antarctic  
698 Circumpolar Current. *Earth and Planetary Science Letters* 235, 715-728.

699 Pfuhl, H.A., Mccave, I.N., Schellenberg, S.A., Ferretti, P., 2004. Changes in Southern Ocean  
700 circulation in late Oligocene to early Miocene time, *The Cenozoic Southern Ocean:*  
701 *Tectonics, Sedimentation, and Climate Change Between Australia and Antarctica.* American  
702 Geophysical Union Washington/DC, pp. 173-189.

703 Prah, F.G., Mix, A.C., Sparrow, M.A., 2006. Alkenone paleothermometry: Biological lessons  
704 from marine sediment records off western South America. *Geochimica et Cosmochimica Acta*  
705 70, 101-117.

706 Prah, F.G., Wakeham, S.G., 1987. Calibration of unsaturation patterns in long-chain ketone  
707 compositions for palaeotemperature assessment. *Nature* 330, 367.

708 Rechka, J., Maxwell, J., 1988. Unusual long chain ketones of algal origin. *Tetrahedron Letters*  
709 29, 2599-2600.

710 Rosell-Melé, A., Carter, J., Eglinton, G., 1994. Distributions of long-chain alkenones and  
711 alkyl alkenoates in marine surface sediments from the North East Atlantic. *Organic*  
712 *Geochemistry* 22, 501-509.

713 Salabarnada, A., Escutia, C., Röhl, U., Nelson, C.H., McKay, R., Jiménez-Espejo, F., Bijl, P.,  
714 Hartman, J., Strother, S., Salzmann, U., 2018. Paleooceanography and ice sheet variability  
715 offshore Wilkes Land, Antarctica–Part 1: Insights from late Oligocene astronomically paced  
716 contourite sedimentation. *Climate of the Past* 14, 991-1014.

717 Scher, H.D., Whittaker, J.M., Williams, S.E., Latimer, J.C., Kordesch, W.E., Delaney, M.L.,  
718 2015. Onset of Antarctic Circumpolar Current 30 million years ago as Tasmanian Gateway  
719 aligned with westerlies. *Nature* 523, 580-583.

720 Stickley, C., Brinkhuis, H., McGonigal, K., Chaproniere, G., Fuller, M., Kelly, D., Nürnberg,  
721 D., Pfuhl, H., Schellenberg, S., Schönfeld, J., 2004a. Late Cretaceous–Quaternary  
722 biomagnetostratigraphy of ODP Sites 1168, 1170, 1171, and 1172, Tasmanian Gateway,  
723 Proceedings of the Ocean Drilling Program, Scientific Results. Ocean Drilling Program,  
724 College Station TX, pp. 1-57.

725 Stickley, C.E., Brinkhuis, H., Schellenberg, S.A., Sluijs, A., Röhl, U., Fuller, M., Grauert, M.,  
726 Huber, M., Warnaar, J., Williams, G.L., 2004b. Timing and nature of the deepening of the  
727 Tasmanian Gateway. *Paleoceanography* 19.

728 Super, J.R., Thomas, E., Pagani, M., Huber, M., O'Brien, C., Hull, P.M., 2018. North Atlantic  
729 temperature and p CO<sub>2</sub> coupling in the early-middle Miocene. *Geology* 46, 519-522.

730 Theroux, S., D'Andrea, W.J., Toney, J., Amaral-Zettler, L., Huang, Y., 2010. Phylogenetic  
731 diversity and evolutionary relatedness of alkenone-producing haptophyte algae in lakes:  
732 implications for continental paleotemperature reconstructions. *Earth and Planetary Science*  
733 *Letters* 300, 311-320.

734 Tierney, J.E., Tingley, M.P., 2015. A TEX(8)(6) surface sediment database and extended  
735 Bayesian calibration. *Sci Data* 2, 150029.

736 Tierney, J.E., Tingley, M.P., 2018. BAYSPLINE: A new calibration for the alkenone  
737 paleothermometer. *Paleoceanography and Paleoclimatology* 33, 281-301.

738 Torsvik, T.H., Steinberger, B., Cocks, L.R.M., Burke, K., 2008. Longitude: linking Earth's  
739 ancient surface to its deep interior. *Earth and Planetary Science Letters* 276, 273-282.

740 Torsvik, T.H., Van der Voo, R., Preeden, U., Mac Niocaill, C., Steinberger, B., Doubrovine,  
741 P.V., Van Hinsbergen, D.J., Domeier, M., Gaina, C., Tohver, E., 2012. Phanerozoic polar  
742 wander, palaeogeography and dynamics. *Earth-Science Reviews* 114, 325-368.

743 van Hinsbergen, D.J., de Groot, L.V., van Schaik, S.J., Spakman, W., Bijl, P.K., Sluijs, A.,  
744 Langereis, C.G., Brinkhuis, H., 2015. A paleolatitude calculator for paleoclimate studies. *PloS*  
745 *one* 10.

746 Villa, G., Persico, D., 2006. Late Oligocene climatic changes: evidence from calcareous  
747 nannofossils at Kerguelen Plateau Site 748 (Southern Ocean). *Palaeogeography,*  
748 *Palaeoclimatology, Palaeoecology* 231, 110-119.

749 Volkman, J.K., Eglinton, G., CoRNER, E.D., Forsberg, T., 1980. Long-chain alkenes and  
750 alkenones in the marine coccolithophorid *Emiliana huxleyi*. *Phytochemistry* 19, 2619-2622.

751 Wei, W., McGonigal, K.L., Zhong, S., 2003. Data report: Paleogene calcareous nannofossil  
752 biostratigraphy of ODP Leg 189 (Australia-Antarctica gateway), Proc. ODP, Sci. Results.  
753 Ocean Drilling Program College Station, TX, p. 114.

754 Westerhold, T., Marwan, N., Drury, A.J., Liebrand, D., Agnini, C., Anagnostou, E., Barnet,  
755 J.S., Bohaty, S.M., De Vleeschouwer, D., Florindo, F., 2020. An astronomically dated record  
756 of Earth's climate and its predictability over the last 66 million years. *Science* 369, 1383-  
757 1387.

758 Young, J.R., 1998. Neogene nannofossils. *Calcareous Nannofossil Biostratigraphy*. Kluwer  
759 Academic, Dordrecht 225, 265.

- 760 Zachos, J.C., Dickens, G.R., Zeebe, R.E., 2008. An early Cenozoic perspective on greenhouse  
761 warming and carbon-cycle dynamics. *Nature* 451, 279-283.
- 762 Zhang, Y.G., Pagani, M., Liu, Z., Bohaty, S.M., Deconto, R., 2013. A 40-million-year history  
763 of atmospheric CO<sub>2</sub>. *Philos Trans A Math Phys Eng Sci* 371, 20130096.
- 764 Zheng, Y., Heng, P., Conte, M.H., Vachula, R.S., Huang, Y., 2019. Systematic  
765 chemotaxonomic profiling and novel paleotemperature indices based on alkenones and  
766 alkenoates: Potential for disentangling mixed species input. *Organic Geochemistry* 128, 26-  
767 41.
- 768 Zheng, Y., Tarozo, R., Huang, Y., 2017. Optimizing chromatographic resolution for  
769 simultaneous quantification of long chain alkenones, alkenoates and their double bond  
770 positional isomers. *Organic Geochemistry* 111, 136-143.
- 771